

Chemical growth of hexagonal zinc oxide nanorods and their optical properties

Pijus Kanti Samanta · Ashok Kumar Bandyopadhyay

Received: 25 July 2011 / Accepted: 25 September 2011 / Published online: 22 November 2011
© The Author(s) 2011. This article is published with open access at Springerlink.com

Abstract A simple wet chemical method has been successfully deployed to fabricate hexagonal zinc oxide nanorods. The structural characteristics were investigated through X-ray diffraction. The crystal unit cell of the nanorods was found to be hexagonal. The morphology of the nanostructures was studied using field emission scanning electron microscopy and transmission electron microscopy. The nanorods are hexagonal in shape. The Zn–O bond formation was confirmed through Fourier transformed infrared spectroscopic analysis. Raman shift measurements revealed various vibrational modes present in the ZnO crystal. The photoluminescence spectrum shows shallow deep level visible emission due to various defect states. Thus, our investigation will be very helpful in the development of ZnO based light emitting/optoelectronic device applications.

Keywords Zinc oxide · Nanorods · Zn–O bond · Raman-shift · Photoluminescence · Visible-emission · Defect-states

Introduction

Zinc oxide (ZnO) is a very well known II–IV semiconductor having interesting unique properties that lead to its applications in sensors, optoelectronic, and nanoelectronic devices (Wang et al. 2006; Song et al. 2010; Umar et al. 2009a, b; Rout et al. 2009). Due to its wide band gap of 3.37 eV and large exciton binding energy of 60 meV (Wang et al. 2009a), it exhibits stable UV emission (Duan

et al. 2006). Researchers reported that visible emission from the ZnO nanostructures originates because of the existence of various defects (Zn interstitial, Zn vacancy, and oxygen vacancy) in the ZnO nanocrystal (Nian et al. 2010; Wang et al. 2009b; Patra et al. 2009). These emissions make ZnO, a very interesting material for various optoelectronic applications. ZnO is now being used as UV absorbing material in sunscreens (Schilling et al. 2010), transparent conductors in solar cells (Lloyd et al. 2009), and nano-lasers (Zhang et al. 2009). Recently Wang (2008) has successfully demonstrated energy generation from arrayed ZnO nanorods using the piezo-electric property exhibited by this material. In addition to these optoelectronic and nanoelectronic device applications, ZnO is also being used in spintronic applications. Existence of ferromagnetism in ZnO was already shown by Iqbal et al. (2009). The idea of this ferromagnetism is now being used in magnetic non-volatile data storage for longer periods of time. Thus, ZnO offers us a possibility to combine the optical and magnetic property in various advanced devices like spin light-emitting-diodes, spin-polarized solar cells, and magneto-optical switching.

In this paper, we report the fabrication of hexagonal ZnO nanorods by a simple and cost-effective wet chemical method. Moreover, it offers us repeated fabrication of pure ZnO. The fabrication is followed by few typical characterization results that are very interesting and useful in ZnO base optoelectronic and nanoelectronic device applications.

Experimental

Material preparation

The chemicals used in the fabrication of ZnO nanorods, were of analytical grade and was used as supplied

P. K. Samanta (✉) · A. K. Bandyopadhyay
Department of Physics, Ghatal Rabindra Satbarsiki
Mahavidyalaya, Ghatal, Paschim Medinipur,
Ghatal 721212, West Bengal, India
e-mail: pijush.samanta@gmail.com

(MERCK) without further purification. 14.87 g of zinc nitrate hexahydrate ($\text{Zn}(\text{NO}_3)_2 \cdot 6\text{H}_2\text{O}$) was dissolved in deionized water to prepare 100 ml solution of concentration 0.5 M. 4 g of sodium hydroxide (NaOH) was dissolved in deionized water to prepare 100 ml NaOH solution of concentration 1 M. This NaOH solution was then put under vigorous stirring at room temperature (34°C) in a conical flask using a magnetic stirrer (SPINOT make). The previously prepared zinc nitrate solution of 0.5 M was added drop-wise to the NaOH solution for 15 min. The mechanical stirring was continued for 2 h. The pH of the solution was 11. A white precipitate was deposited at the bottom of the flask. The precipitate was then filtered and washed 2–3 times with distilled water. Then the powdered sample was dried and annealed at different temperatures (200, 400, and 800°C) in a furnace for further characterizations.

Material characterization

The X-ray diffraction (XRD) data were collected in a RIGAKU diffractometer using Cu K_α -radiation over an angular range $30^\circ < 2\theta < 60^\circ$ by an ionization chamber. The morphology of the samples were observed using ZEISS SUPRA-40 field emission scanning electron microscope (FESEM) operating at 5 kV accelerating voltage and the working distance between the samples and the detector was ~ 1.5 cm. Transmission electron microscopy (TEM) was carried out in a JEOL JEM-2100F microscope with the accelerating voltage of 200 kV. For TEM study, a very small amount of the powder sample was first dispersed in acetone by ultrasonication. A drop of that solution was taken on a carbon coated grid and dried in vacuum for TEM imaging. Fourier transformed infra-red spectroscopy (FTIR) was carried out in NEXUS-870 FT-IR spectrometer. Reinshaw Raman system: RM-1000B (coupled with LEICA microscope DMLM) was deployed to carry out the Raman shift measurement of the ZnO nanorods. As the excitation source, a 20 mW Argon ion laser was used which was operated at 514 nm wavelength using an edge filter of 200 cm^{-1} as cut-off. The optical emission characteristic of the ZnO nanorods was analysed by recording the photoluminescence (PL) spectrum at room temperature using PERKIN ELMER LS-55 luminescence spectrometer with a xenon lamp at the excitation of 325 nm.

Results and discussions

X-ray diffraction (XRD)

A typical XRD pattern of the ZnO nanorods annealed at 400°C is shown in Fig. 1. The unit cell of the crystal was found to be hexagonal with the presence of the peaks (100),

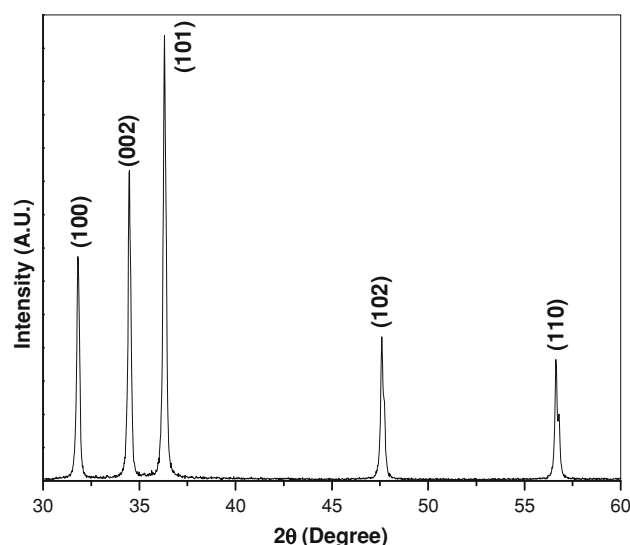
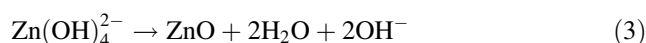
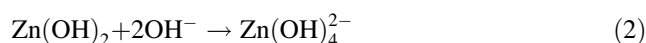
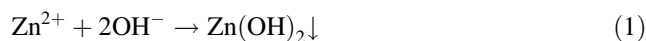


Fig. 1 XRD pattern of ZnO nanorods annealed at 400°C

(002), (101), (102), and (110). It is well agreed with the standard JCPDS card no. 36-1451. Furthermore, the intensities of different diffraction peaks are different, which indicates that the growth of various planes (direction) is different and that the growth is anisotropic. The crystallite size was calculated using the well known Scherer formula (Samanta and Chaudhuri 2011): $R_{\text{hkl}} = \frac{0.89\lambda}{\beta \cos \theta}$. In this calculation, the highest intensity (101) peak was analysed and considered it to be Gaussian. The crystallite size was found to be 43 nm. Besides, no impurity peaks were detected which indicates that the fabricated ZnO nanomaterials is highly pure.

Growth and morphology of the nanostructures

Typical FESEM image of the as prepared ZnO nanorods is shown in Fig. 2a. Rod-like nanostructures were clearly observed. The nanorods are randomly distributed in the powdered sample. The length of the nanorods is ~ 400 nm and diameter is ~ 100 nm. Growth of various ZnO nanostructures from aqueous solution (containing $\text{Zn}(\text{OH})_4^{2-}$) has been reported by many researchers. However, the growth process and mechanism of the formation of ZnO from $\text{Zn}(\text{OH})_4^{2-}$ is not yet well understood. The reported mechanism of formation of ZnO by researchers (Li et al. 2007; Kale et al. 2007; Hu et al. 2007; Quang et al. 2005; Shan et al. 2004; Zhang et al. 2002; Wu et al. 2006; Samanta et al. 2009a) is as follows:



We depict the formation mechanism of ZnO nanorods in two steps: nucleation and growth. At the initial step of the

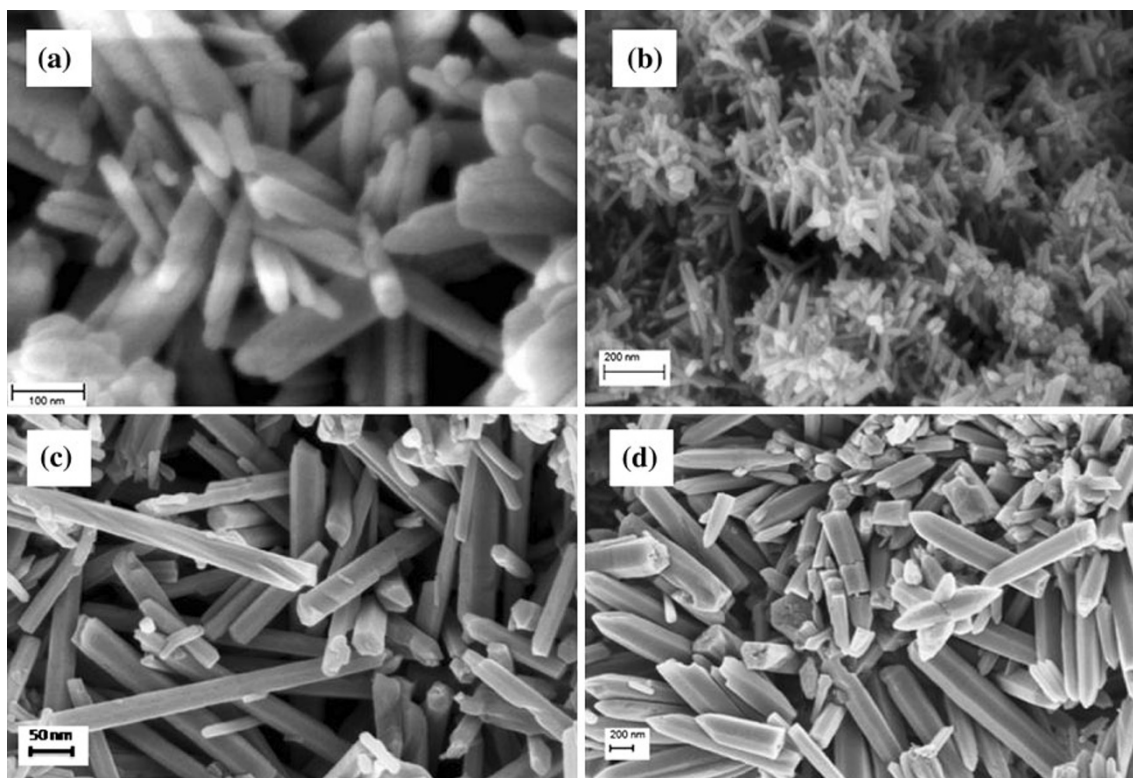
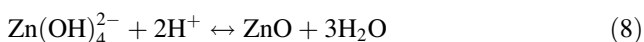
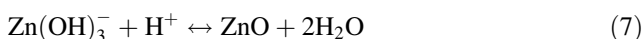
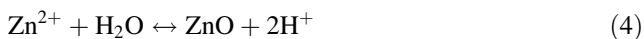


Fig. 2 FESEM images of the **a** as synthesized ZnO nanorods, and ZnO nanorods annealed at **b** 200°C, **c** 400°C, and **d** 800°C, respectively

reaction between $\text{Zn}(\text{OH})_2$ and NaOH , $\text{Zn}(\text{OH})_2$ precipitates. Now as more NaOH is added to the solution, the precipitated $\text{Zn}(\text{OH})_2$ dissolves and forms a homogeneous aqueous solution that contains enough $\text{Zn}(\text{OH})_4^{2-}$ ions. At the onset of supersaturation and dehydration of $\text{Zn}(\text{OH})_4^{2-}$ ZnO nuclei are formed. It is also supposed that during this process, $\text{Zn}(\text{OH})_4^{2-}$ ions act as the growth unit of ZnO and directly incorporated into ZnO crystallites. These nuclei grow further to produce rod-like ZnO. However, there are also some other equilibrium processes ($\text{ZnO}-\text{H}_2\text{O}$) for the formation of ZnO as reported by Quang et al. (2005). But these needs further investigations.



The wurtzite structure of ZnO can be described as a stack of a number of alternating planes that are fourfold co-ordinated O^{2-} and Zn^{2+} ions arranged along c -axis. Several crystal planes exist: the basal plane (0001), one end of this plane is terminated to Zn lattice points and (000 $\bar{1}$) plane terminates to negative oxygen lattice points (Sugunan et al. 2006). The other six low index non-polar

facets ($\bar{1}010$) are parallel to c -axis. The non-polar facets are energetically most stable and the polar facets are metastable (Pan et al. 2001). The growth rate of various planes follows the growth rule: $V(0001) > V(01\bar{1}\bar{1}) > V(01\bar{1}0) > V(01\bar{1}1) > V(000\bar{1})$ (Li et al. 1999). Now the growth rate of (0001) plane is very high. As a result it will be disappeared quickly. Thus, this plane disappears in the experimentally synthesized ZnO leading to the rod-like structure (Li et al. 1999). A more detailed understanding of the growth rate dependence of various morphologies of ZnO nanostructures is reported by Li et al. (1999). Schematic of the growth of the nanorods is shown in Fig. 3. On annealing the nanorods at higher temperatures, the small crystallites coalesce together to form large crystallites and the crystallinity of the material improves, and hence defect states are reduced. Hence shape evolution occurs. There are possibilities of hydroxide shell surrounding the as-synthesized nanorods. But high temperature annealing will remove these hydroxide shell layers. As a result well-grown hexagonal nanorods with narrow tips were observed as shown in Fig. 2b–d).

Transmission electron microscopy (TEM) study

Typical TEM image of the nanorods annealed at 400°C is shown in Fig. 4a, b. We observed rod-like structures with diameter ~ 50 – 100 nm and length ~ 400 nm as measured

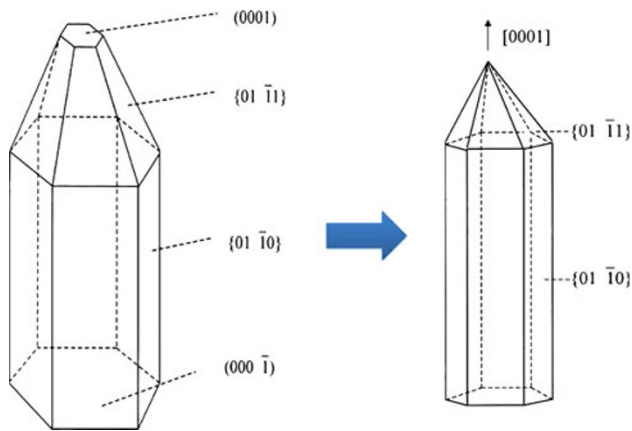


Fig. 3 Schematic of the growth of the nanorods [reproduced with permission from 27]

from TEM image. The crystallite size (43 nm) is less than the diameter of the nanorods, which indicates the nanorods are composed of several crystallites. The selected area electron diffraction (SAED) pattern is also shown in the inset of Fig. 4b. The linear diffraction points indicate that the diffraction occurs from a single crystallite within the nanorods.

Fourier transformed infra-red spectroscopy

Figure 5 shows the FTIR spectrum of the ZnO nanorods. A very strong band is observed at $\sim 500 \text{ cm}^{-1}$. This is assigned to the Zn–O stretching bonds (Faal Hamedani and Farzaneh 2006). Another peak at $1,625 \text{ cm}^{-1}$ arises due to the O–H bending mode of water. The vibration mode of OH group was also observed at $3,429 \text{ cm}^{-1}$. It revealed

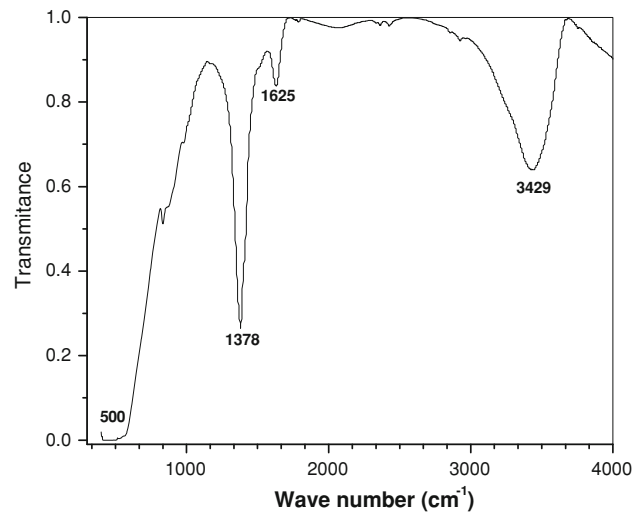


Fig. 5 FTIR spectrum of the ZnO nanorods showing the absorption for various bonds

that some water was absorbed by the sample from the atmosphere. The peak at $1,378 \text{ cm}^{-1}$ appeared due to symmetric stretching mode of N = O coming from some unreacted zinc nitrate.

Raman shift measurement

Chemical growth of nanostructured materials usually involves the formation of large amount of surface defects in the nanocrystals. Thus, the Raman spectra of these chemically grown nanomaterials are red shifted and broadened due to the relaxation of the selection rule for the q -vector (conservation of crystal momentum) within the finite size of the nanocrystals. Also the phonon scattering in

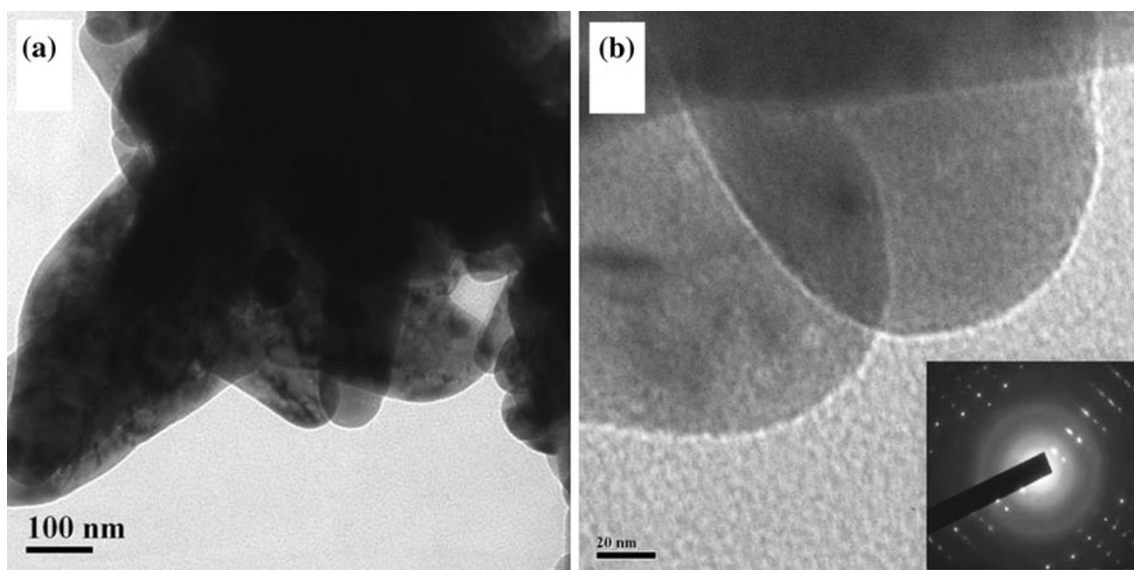


Fig. 4 a, b TEM images of the nanorods annealed at 400°C . Inset shows the SAED pattern

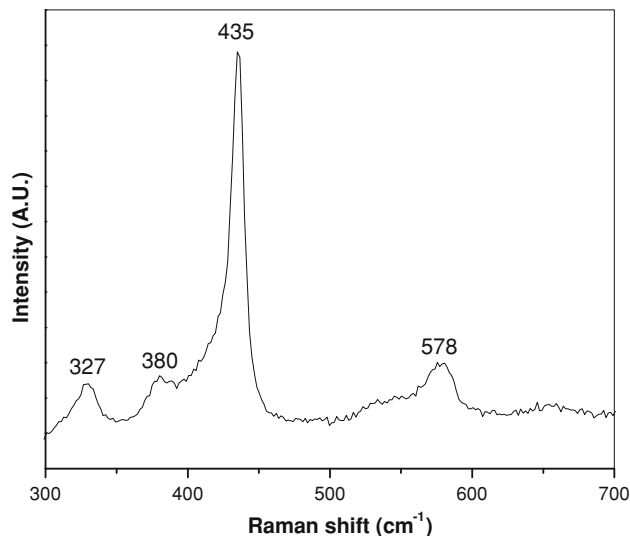


Fig. 6 Raman shift measurements of the nanorods

this case are no longer limited to the Brillouin zone center but dispersed around the centre of the Brillouin zone. This result in the appearance of symmetry forbidden modes along with the shifting and broadening of the first-order optical phonon scattering modes. ZnO has hexagonal crystal structure with space group C_{6v}^4 . The Raman-active modes for hexagonal ZnO are $A_1 + 2E_2 + E_1$. The polar modes A_1 and E_1 can split into transverse optical (TO) and longitudinal optical (LO) modes. The nonpolar E_2 mode is composed of two modes with a low and high frequency. Figure 6 shows the Raman spectra of the ZnO nanorods. Prominent vibration peaks at 327, 380, 435, and 578 cm^{-1} were observed. The 578 cm^{-1} peak, positioned between A_1 (LO) and E_1 (LO) optical phonon mode, arises due to the oxygen deficiency. It is in good agreement with the theoretical calculations of Fonoberov and Balandin (2004). As a result existence of oxygen deficiency, we also observe PL emission peak at ~ 527 nm. The nonpolar E_2 mode is observed at 435 cm^{-1} (Alim et al. 2005; Samanta et al. 2010). The peak at 381 cm^{-1} is attributed to A_1 transverse mode and arises due to the anisotropy in the force constant. It has a different frequency from E_1 transverse phonon mode. The 327 cm^{-1} peak is due to the second order Raman process and is assigned to the $2E_2$ mode (Fonoberov and Balandin 2004; Alim et al. 2005).

Photoluminescence spectroscopy

Typical PL spectra of the ZnO nanorods annealed at different temperatures are shown in Fig. 7. UV emission is the characteristic emission of ZnO arising due to direct band transition. However, visible emission is also reported from ZnO nanostructures owing to various defects (Samanta and Chaudhuri 2011; Samanta et al. 2009a, b, c; Vanheusden

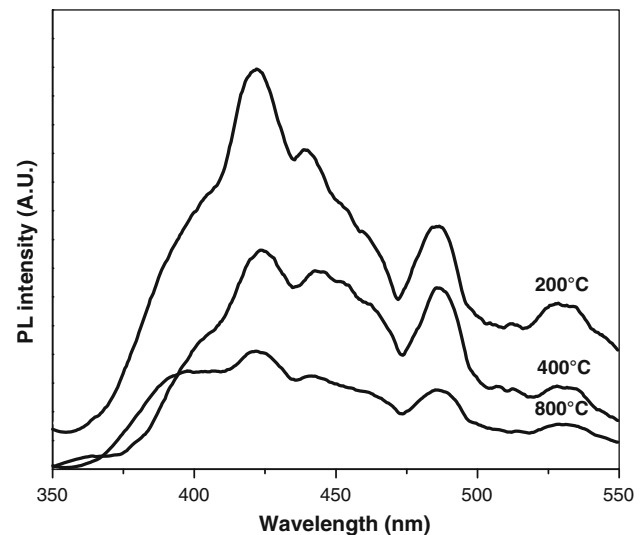


Fig. 7 Room temperature PL spectrum from ZnO nanorods annealed at different temperatures

et al. 1996; Jeong et al. 2003; Jin et al. 2000; Fu et al. 1998) such as oxygen vacancies, Zn interstitials, etc. Oxygen, in general, exhibits three types of charge states of oxygen vacancies such as Vo^0 , Vo^+ , and Vo^{2+} . The oxygen vacancies are located below the bottom of the conduction band (CB) in the sequence of Vo^0 , Vo^+ , and Vo^{2+} , from top to bottom. Shallow acceptor levels are created at 0.3 and 0.4 eV above the top of the valence band (VB) due to zinc vacancy (V_{Zn}) and oxygen interstitial (O_i), respectively. Again, zinc interstitial (Zn_i) produces a shallow donor level at 0.5 eV below the bottom of CB (Samanta and Chaudhuri 2011; Samanta et al. 2009a, b, c; Vanheusden et al. 1996; Jeong et al. 2003; Jin et al. 2000; Fu et al. 1998). In our cases, we observed PL emission (see Fig. 7) in the visible region which indicates that the PL emission from the nanorods in this case is dominated by the defect related deep level emission over the band edge UV emission. Various defect energy levels as calculated from full potential linear Muffin-Tin orbital method (Vanheusden et al. 1996; Jeong et al. 2003; Jin et al. 2000; Fu et al. 1998; Samanta et al. 2009b, c; Lin et al. 2011; Xu et al. 2003) are shown in Fig. 8. The peak at 405 nm (3.06 eV) corresponds to the transition between conduction band and vacancy zinc level while the peak at 425 nm (2.92 eV) corresponds to the recombination between electron at zinc interstitials and hole in the valence band (Vanheusden et al. 1996; Jeong et al. 2003; Jin et al. 2000; Fu et al. 1998; Samanta et al. 2009b, c; Lin et al. 2011; Xu et al. 2003). The peak at 485 nm (2.55 eV) arises due to transition between zinc interstitial and zinc vacancy level. The peak around 527 nm can be related to singly ionized oxygen vacancy (Vanheusden et al. 1996). This green emission at

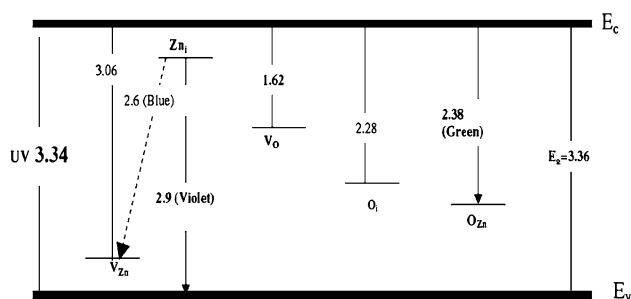


Fig. 8 Defect levels in ZnO

527 nm (2.35 eV) is the result of the recombination of a photo-generated hole with a singly ionized charged state of the specific defect. For better understanding of the correlation between PL emission and interstitial Zn, we observed the PL spectra of the samples annealed at 200, 400 and 800°C, respectively. At high temperature annealing, the small crystallites coalesce together to form large crystallites and the crystallinity of the material improves. This leads to decrease in interstitial zinc states in the nanocrystals resulting less transitions. Hence at higher annealing temperature the intensity of the visible emission peak at 425 nm from ZnO nanorods is reduced.

For better understanding of the PL emission mechanism, we studied the low temperature PL spectra of the fabricated ZnO nanorods over the temperature range of 10–300 K as shown in Fig. 9. Very sharp peak around 3.36 eV appeared and is assigned to donor-bound excitons (D^0X) (Mandal et al. 2008; Vaithianathan et al. 2005; Reynolds et al. 2001; Meyer et al. 2004). Another PL peak of very high intensity appeared at ~ 3.22 eV owing to zero-phonon transition (Mandal et al. 2008; Vaithianathan et al. 2005; Reynolds

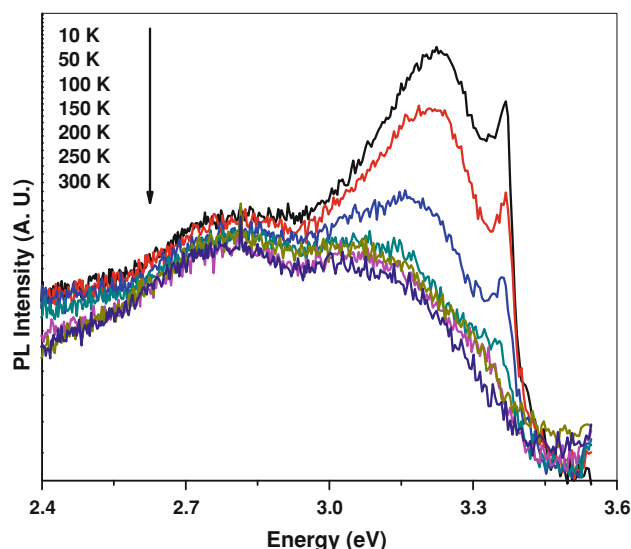


Fig. 9 Low temperature PL spectrum of ZnO nanorods

et al. 2001). However, Meyer et al. (2004) reported that this PL peak is due to donor–acceptor pair transition. It is also reported that the defect-related PL emission dominates for the nanorods of high-aspect ratio as compared to that of bulk because of more number of surface states and incorporation of impurities. However, there are some reports of strong bound excitonic peak at a temperature below 20 K for ZnO bulk single crystal (Park et al. 2003). In our case, the room temperature PL is dominated by the defect state emission.

Conclusions

Hexagonal ZnO nanorods have been fabricated by a wet chemical process. The fabricated nanorods are well crystallized as revealed from the XRD data. FTIR and Raman shift measurements confirmed various vibrational bonds of the ZnO. A strong violet emission at 425 nm was observed from the nanorods. This violet emission is very rare finding in ZnO nanostructures. This violet emission occurs due to the recombination of electrons at zinc interstitials and holes in the valence band. Thus, the fabricated ZnO nanomaterial can be used as a violet light emitting material and may find its applications in optoelectronic devices.

Acknowledgments The authors sincerely thank Prof. P. R. Chaudhuri and CRF-IIT Kharagpur for providing the FESEM, TEM and FTIR measurements. The authors are also thankful to Prof. S. K. Roy for providing the low temperature PL facility. The authors also acknowledge the financial support provided by Ghatal R. S. Mahavidyalaya to carry out this work.

Open Access This article is distributed under the terms of the Creative Commons Attribution License which permits any use, distribution and reproduction in any medium, provided the original author(s) and source are credited.

References

- Alim KA, Fonoberov VA, Shamsa M, Balandin AA (2005) Micro-Raman investigation of optical phonons in ZnO nanocrystals. *J Appl Phys* 97:124313(1)–124313(6)
- Duan L, Lin B, Zhang W, Zhong S, Fu Z (2006) Enhancement of ultraviolet emissions from ZnO films by Ag doping. *Appl Phys Lett* 88:232110(1)–232113(3)
- Faal Hamedani N, Farzaneh F (2006) Islamic Republic of Iran. *J Sci* 17:231
- Fonoberov VA, Balandin AA (2004) Interface and confined optical phonons in wurtzite nanocrystals. *Phy Rev B* 70:233205(1)–233205(4)
- Fu ZX, Guo CX, Lin BX, Liao GH (1998) Cathodoluminescence of ZnO Films. *Chin Phys Lett* 15:457–459
- Hu H, Huang X, Deng C, Chen X, Qian Y (2007) Hydrothermal synthesis of ZnO nanowires and nanobelts on a large scale. *Mater Chem Phys* 106:58–62

- Iqbal J, Baiqi W, Liu X, Huichao Z, Dapeng Y, Ronghai Y (2009) Role of sp-d exchange interactions in room-temperature photoluminescence and ferromagnetism of CuCo Co-doped ZnO nanorods. *J Nanosci Nanotechnol* 9:6823–6827
- Jeong SH, Kim BS, Lee BT (2003) Photoluminescence dependence of ZnO films grown on Si(100) by radio-frequency magnetron sputtering on the growth ambient. *Appl Phys Lett* 82:2625(1)–2625(3)
- Jin BJ, Im S, Lee SY (2000) Violet and UV luminescence emitted from ZnO thin films grown on sapphire by pulsed laser deposition. *Thin Solid Films* 366:107–110
- Kale RB, Hsu Y, Lin Y, Lu S (2007) Synthesis of stoichiometric flowerlike ZnO nanorods with hundred per cent morphological yield. *Solid State Commun* 142:302–305
- Li W, Shi E, Zhong W, Yin Z (1999) Growth mechanism and growth habit of oxide crystals. *J Cryst Growth* 203:186–196
- Li P, Liu H, Zhang Y, Wei Y, Wang X (2007) Synthesis of flowerlike ZnO microstructures via a simple solution route. *Mater Chem Phys* 106:63–69
- Lin B, Fu Z, Jia Y (2011) Green luminescent center in undoped zinc oxide films deposited on silicon substrates. *Appl Phys Lett* 79:943(1)–943(3)
- Lloyd MT, Lee YJ, Davis RJ, Fang E, Fleming RM, Hsu JWP (2009) Improved efficiency in Poly(3-hexylthiophene)/zinc oxide solar cells via lithium incorporation. *J Phys Chem C* 113:17608–17612
- Mandal S, Mullick H, Dhar A, Ray SK (2008) Self-assembled growth of hexagonal ZnO nanoprisms exhibiting good photoluminescence property. *J Electrochem Soc* 155:K129–K132
- Meyer BK, Alves H, Hofmann DM, Kriegseis W, Forster D, Bertram F, Christen J, Hoffmann A, Strahburg M, Dworzak M, Habocek U, Rodina AV (2004) Bound exciton and donor–acceptor pair recombinations in ZnO. *Phys Status Solidi B Basic Res* 241: 231–260
- Nian H, Hahn SH, Koo KK, Kim JS, Kim S, Shin EW, Kim EJ (2010) Preparation and characterization of sol–gel Li and Al codoped ZnO thin films. *Mater Lett* 64:157–160
- Pan ZW, Dai ZR, Wang ZL (2001) Nanobelts of semiconducting oxides. *Science* 291:1947–1949
- Park WI, Jun YH, Jung SW, Yi G (2003) Excitonic emissions observed in ZnO single crystal nanorods. *Appl Phys Lett* 82:964(1)–964(3)
- Patra MK, Manoth M, Singh VK, Gowd GS, Choudhry VS, Vadera SR, Kumar N (2009) Synthesis of stable dispersion of ZnO quantum dots in aqueous medium showing visible emission from bluish green to yellow. *J Lumin* 129:320–324
- Quang HL, Chua SJ, Loh KP, Zhen C, Thompson CV, Fitzgerald E (2005) The effect of post-annealing treatment on photoluminescence of ZnO nanorods prepared by hydrothermal synthesis. *Adv Mater Micro Nanosyst* 1:1–4
- Reynolds DC, Look DC, Jogai B, Collins TC (2001) Polariton and free-exciton-like photoluminescence in ZnO. *Appl Phys Lett* 79:3794(1)–3794(3)
- Rout CS, Kulkarni GU, Rao CNR (2009) Electrical and hydrogen-sensing characteristics of field effect transistors based on nanorods of ZnO and WO. *J Nanosci Nanotechnol* 9:5652–5658
- Samanta PK, Chaudhuri PR (2011) Growth and optical properties of chemically grown ZnO nanobelts. *Sci Adv Mater* 3:107–112
- Samanta PK, Patra SK, Chaudhuri PR (2009a) Violet emission from flower-like bundle of ZnO nanosheets. *Physica E* 41:664–667
- Samanta PK, Patra SK, Chaudhuri PR (2009b) Visible emission from ZnO nanorods synthesized by a simple wet chemical method. *Int J Nanosci Nanotechnol* 1:81–90
- Samanta PK, Patra SK, Chaudhuri PR (2009c) Green photoluminescence from chemically synthesized ZnO nanostructure. *Int J Mater Sci* 4:803–806
- Samanta PK, Bandyopadhyay AK, Basak S, Chaudhuri PR (2010) Characteristics of electrochemically grown dendritic metallic zinc. *Int J Light Electron Opt* 122:1520–1522
- Schilling K, Bradford B, Castelli D, Dufour E, Nash JF, Pape W, Schulte S, Tooley L, Bosch JV, Schellauf F (2010) Human safety review of “nano” titanium dioxide and zinc oxide. *Photochem Photobiol Sci* 9:495–509
- Shan FK, Shin BC, Jang SW, Yu YS (2004) Substrate effects on ZnO thin films prepared by PLD technique. *J Eur Ceram Soc* 24:1015–1018
- Song HS, Zhang WJ, Tang YB, He ZB, Yuan GD, Fan X, Lee CS, Bello I, Lee ST (2010) Field electron emission of ZnO nanowire pyramidal bundle arrays. *J Nanosci Nanotechnol* 10:2360–2365
- Sugunan A, Warad HC, Boman M, Dutta J (2006) Zinc oxide nanowires in chemical bath on seeded substrates: role of hexamine. *J Sol–Gel Sci Technol* 39:49–56
- Umar A, Park YK, Hahn YB (2009a) High aspect-ratio ZnO nanowires based nanoscale field effect transistors. *J Nanosci Nanotechnol* 9:2692–2697
- Umar A, Rahman MM, Hahn YB (2009b) ZnO nanorods based hydrazine sensors. *J Nanosci Nanotechnol* 9:4686–4691
- Vaithianathan V, Lee BT, Kim SK (2005) Preparation of As-doped p-type ZnO films using a Zn₃As₂/ZnO target with pulsed laser deposition. *Appl Phys Lett* 86:062101(1)–062101(3)
- Vanheusden K, Seager CH, Warren WL, Tallant DR, Voigt JA (1996) Correlation between photoluminescence and oxygen vacancies in ZnO phosphors. *Appl Phys Lett* 68(3):403(1)–403(3)
- Wang ZL (2008) Towards self-powered nanosystems: from nanogenerators to nanopiezotronics. *Adv Funct Mater* 18:3553–3567
- Wang XD, Zhou J, Song J, Liu J, Xu N, Wang ZL (2006) Piezoelectric field effect transistor and nanoforce sensor based on a single ZnO nanowire. *Nano Lett* 6(12):2768–2772
- Wang WS, Wu TT, Chou TH, Chen YY (2009a) A ZnO nanorod-based SAW oscillator system for ultraviolet detection. *Nanotechnology* 20:135503
- Wang M, Cheng X, Yang J (2009b) Controlled visible photoluminescence of ZnO thin films prepared by RF magnetron sputtering. *Appl Phys A Mater Sci Process* 96:783–787
- Wu X, Bai H, Li C, Shi G (2006) Controlled one-step fabrication of highly oriented ZnO nanoneedle/nanorods arrays at near room temperature. *Chem Commun* 15:1655–1657
- Xu PS, Sun YM, Shi CS, Xu FQ, Pan HB (2003) The electronic structure and spectral properties of ZnO and its defects. *Nucl Instrum Methods Phys Res Sect B* 199:286–290
- Zhang J, Sun L, Yin J, Su H, Liao C, Yan C (2002) Control of ZnO morphology via a simple solution route. *Chem Mater* 14:4172–4177
- Zhang C, Zhang F, Xia T, Kumar N, Hahn J, Liu J, Wang ZL, Xu J (2009) Low-threshold two-photon pumped ZnO nanowire lasers. *Opt Express* 17:7893–7900